**Supporting Information**

# Luminescent behaviour of Au(I)-Cu(I) heterobimetallic coordination polymers based on alkynyl-tris(2-pyridyl)phosphine Au(I) complexes

Stanislav K. Petrovskii[a], Aleksandra V. Paderina[a], Anastasia A. Sizova[a], Andrey Yu. Baranov[b], Alexander A. Artem'ev[b], Vladimir V. Sizov[a*] and Elena V. Grachova[a*]

[a] Institute of Chemistry, St. Petersburg State University, Universitetskiy pr. 26, 198504 St. Petersburg, Russia

[b] Nikolaev Institute of Inorganic Chemistry, Siberian Branch of Russian Academy of Sciences, Acad. Lavrentiev Ave. 3, 630090 Novosibirsk, Russia

E-mail: e.grachova@spbu.ru

sizovvv@mail.ru

**Content of Supporting Information**

**Table S1**. Crystallographic data for **1**, **2**, and **4a**.

| | **1** | **2** | **4a** |
|---|---|---|---|
| Formula | $C_{23}H_{17}AuN_3P$ | $C_{30}H_{24}AuN_3OP$ | $C_{144}H_{111}Au_6B_6Cu_6F_{24}N_{21}P_6$ |
| Crystal System | Monoclinic | Triclinic | Hexagonal |
| *a* (Å) | 8.5575(3) | 10.4121(5) | 15.2140(2) |
| *b* (Å) | 10.8642(5) | 11.9530(5) | 15.2140(2) |
| *c* (Å) | 21.2885(8) | 12.0119(5) | 19.3663(2) |
| $\alpha$ (°) | 90 | 109.897(4) | 90 |
| $\beta$ (°) | 91.365(4) | 111.317(4) | 90 |
| $\gamma$ (°) | 90 | 100.110(4) | 120 |
| *V* (Å$^3$) | 1978.64(14) | 1230.74(11) | 3882.07(11) |
| Molecular weight | 563.33 | 669.46 | 4405.34 |
| Space group | $P2_1/c$ | P-1 | $P3_221$ |
| $\mu$ (mm$^{-1}$) | 7.529 | 6.071 | 12.535 |
| Temperature (K) | 100(11) | 100(11) | 100.00(11) |
| *Z* | 4 | 2 | 6 |
| $D_{calc}$ (g/cm$^3$) | 1.891 | 1.809 | 1.901 |
| Crystal size (mm$^3$) | 0.412 × 0.348 × 0.231 | 0.302 × 0.254 × 0.037 | 0.365 × 0.306 × 0.237 |
| Diffractometer | Xcalibur Eos | Xcalibur Eos | XtaLAB HyPix-3000 |
| Radiation | Mo*K*α | Mo*K*α | Cu*K*α |
| Total reflections | 9326 | 11477 | 36133 |
| Unique reflections | 4529 | 6807 | 5133 |
| Angle range 2$\theta$ (°) | 5.358–54.996 | 5.72–61.784 | 6.708–144.996 |
| Reflections with $\|F_o\| \geq 4\sigma_F$ | 3617 | 6282 | 5008 |
| $R_{int}$ | 0.0518 | 0.0330 | 0.0391 |
| $R_\sigma$ | 0.0767 | 0.0602 | 0.0198 |
| $R_1$ ($\|F_o\| \geq 4\sigma_F$) | 0.0398 | 0.0300 | 0.0340 |
| $wR_2$ ($\|F_o\| \geq 4\sigma_F$) | 0.0690 | 0.0596 | 0.0902 |
| $R_1$ (all data) | 0.0552 | 0.0341 | 0.0349 |
| $wR_2$ (all data) | 0.0767 | 0.0620 | 0.0922 |
| *S* | 1.018 | 1.051 | 1.154 |
| $\rho_{min}$, $\rho_{max}$, *e*/Å$^3$ | –1.67, 2.14 | –1.38, 1.75 | –1.08, 2.42 |
| CCDC | 2012566 | 2012565 | 2012567 |

$R_1 = \Sigma||F_o| - |F_c||/\Sigma|F_o|$; $wR_2 = \{\Sigma[w(F_o^2 - F_c^2)^2]/\Sigma[w(F_o^2)^2]\}^{1/2}$; $w = 1/[\sigma^2(F_o^2)+(aP)^2 + bP]$, where $P = (F_o^2 + 2F_c^2)/3$; $s = \{\Sigma[w(F_o^2 - F_c^2)]/(n - p)\}^{1/2}$ where *n* is the number of reflections and *p* is the number of refinement parameters.

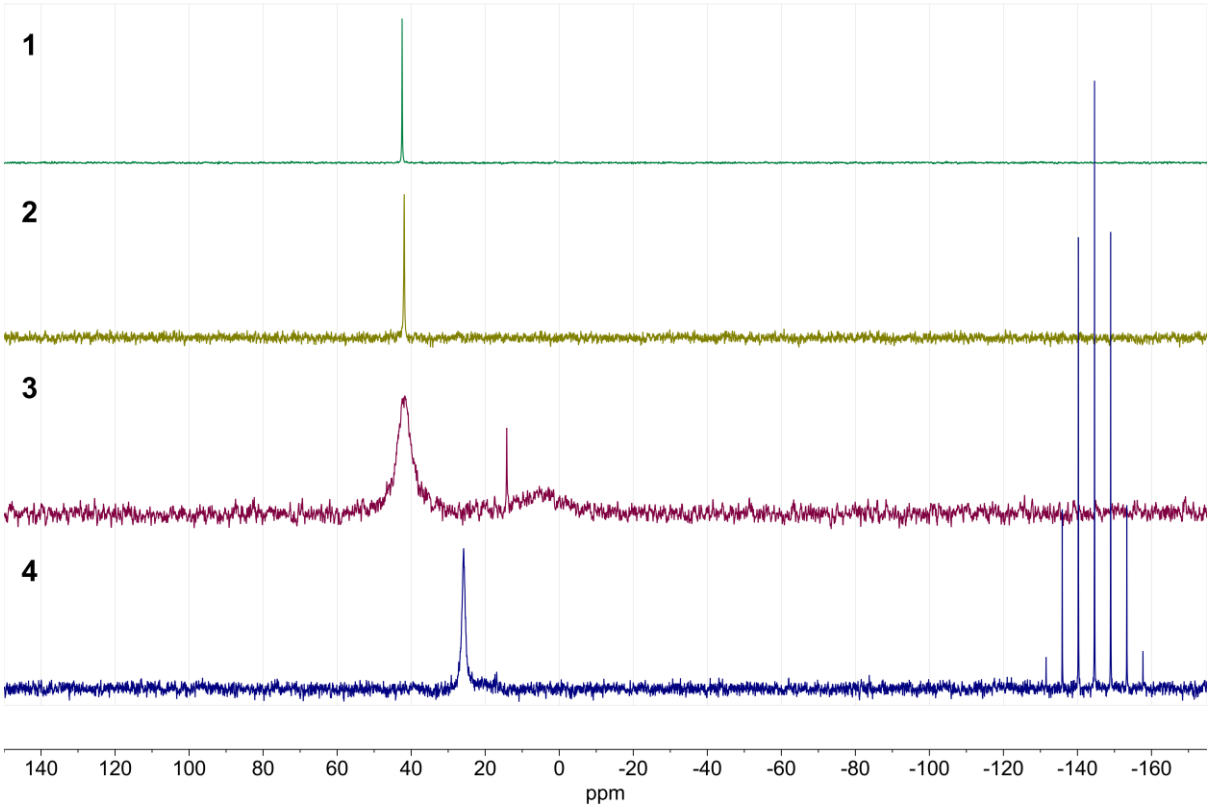


**Figure S1.** $^{31}P\{^{1}H\}$ NMR spectra of **1**, **2** ($(CD_3)_2CO$), **3** ($CDCl_3$), and **4** ($CD_3CN$), r.t.

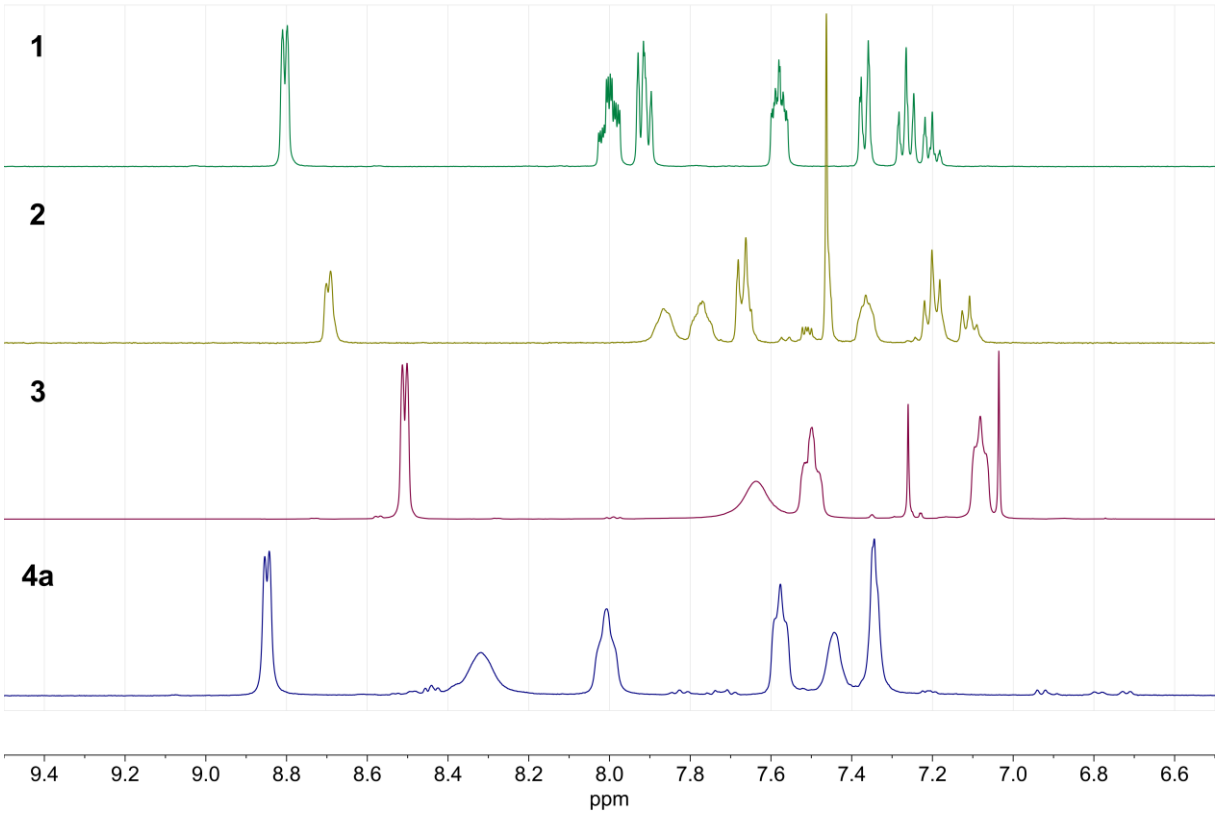


**Figure S2.** $^{1}H$ NMR spectra of **1**, **2** ($(CD_3)_2CO$), **3** ($CDCl_3$), and **4a** ($CD_3CN$), aromatic region, r.t.

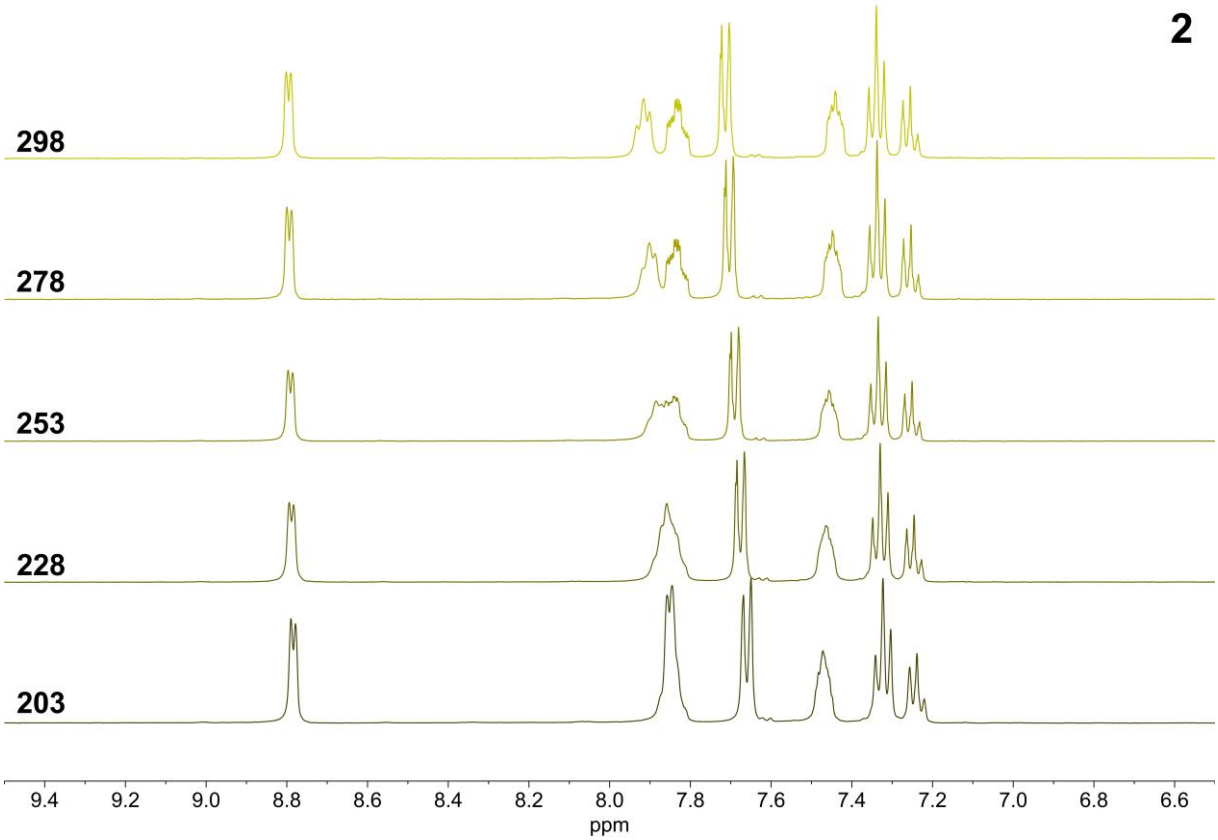


**Figure S3.** Variable temperature $^{1}$H NMR spectra of **2**, $CD_2Cl_2$, aromatic region. The temperature is indicated in K.

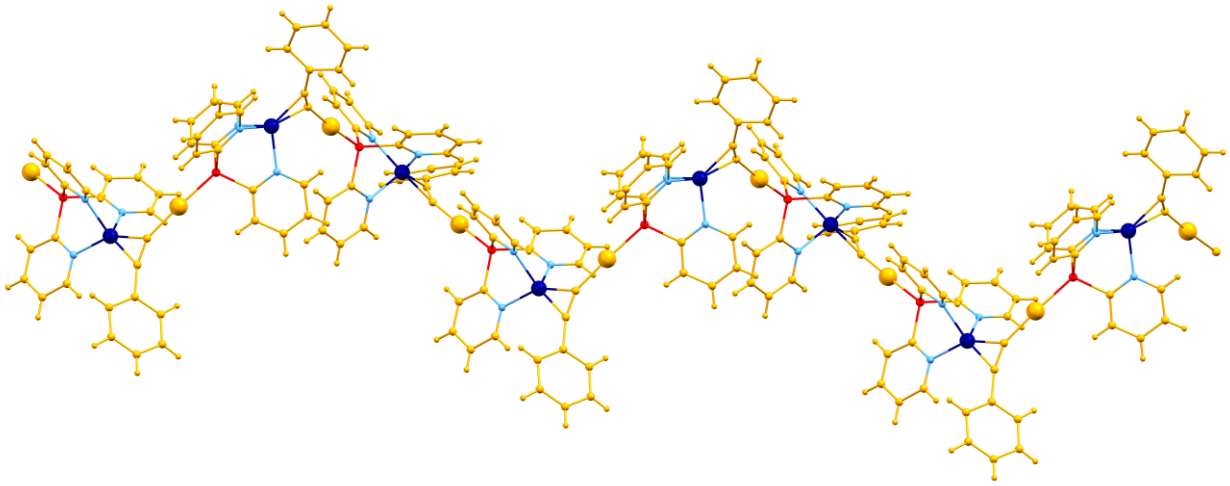

**Figure S4.** Solid state structure of **4a** ($BF_4^-$ anions are omitted for clarity). Colour legend: coper is indigo, phosphorous is red, nitrogen is light blue, all other atoms are orange.

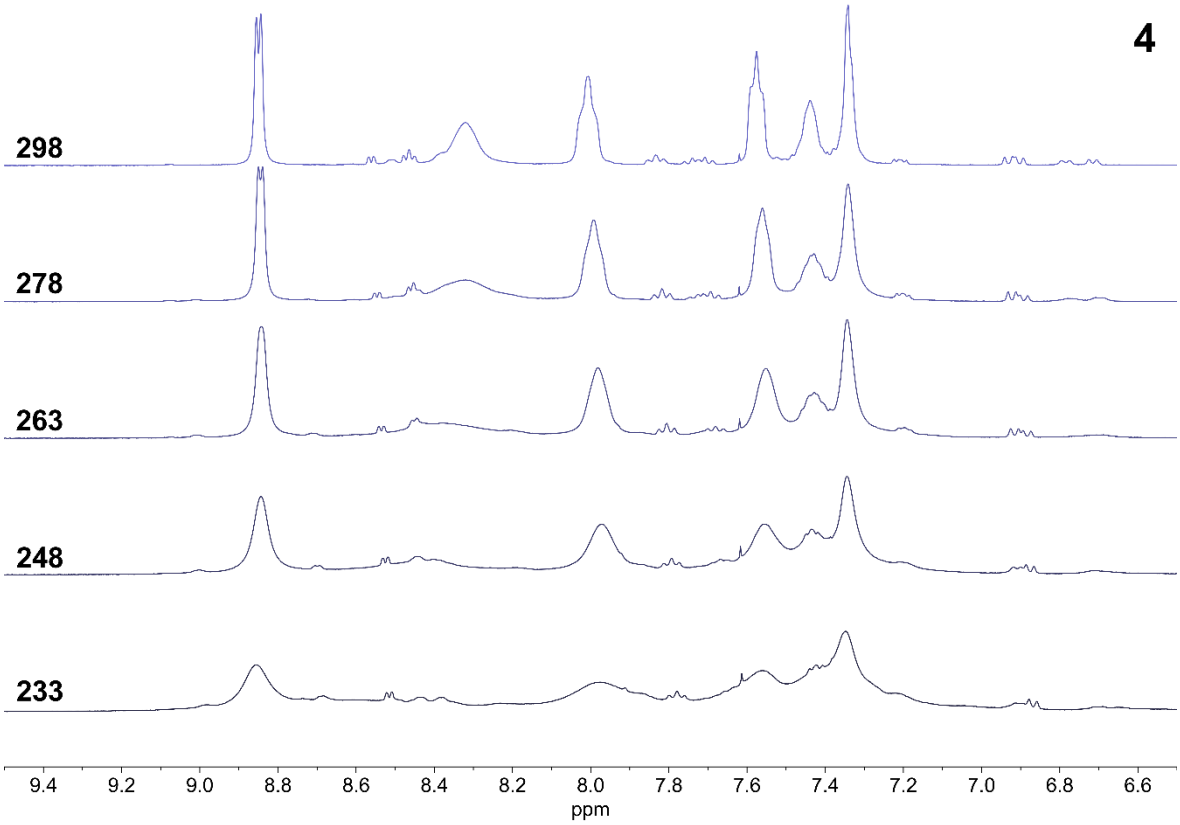


**Figure S5.** Variable temperature $^{1}$H NMR spectra of **4**, $CD_3CN$, aromatic region. The temperature is indicated in K.

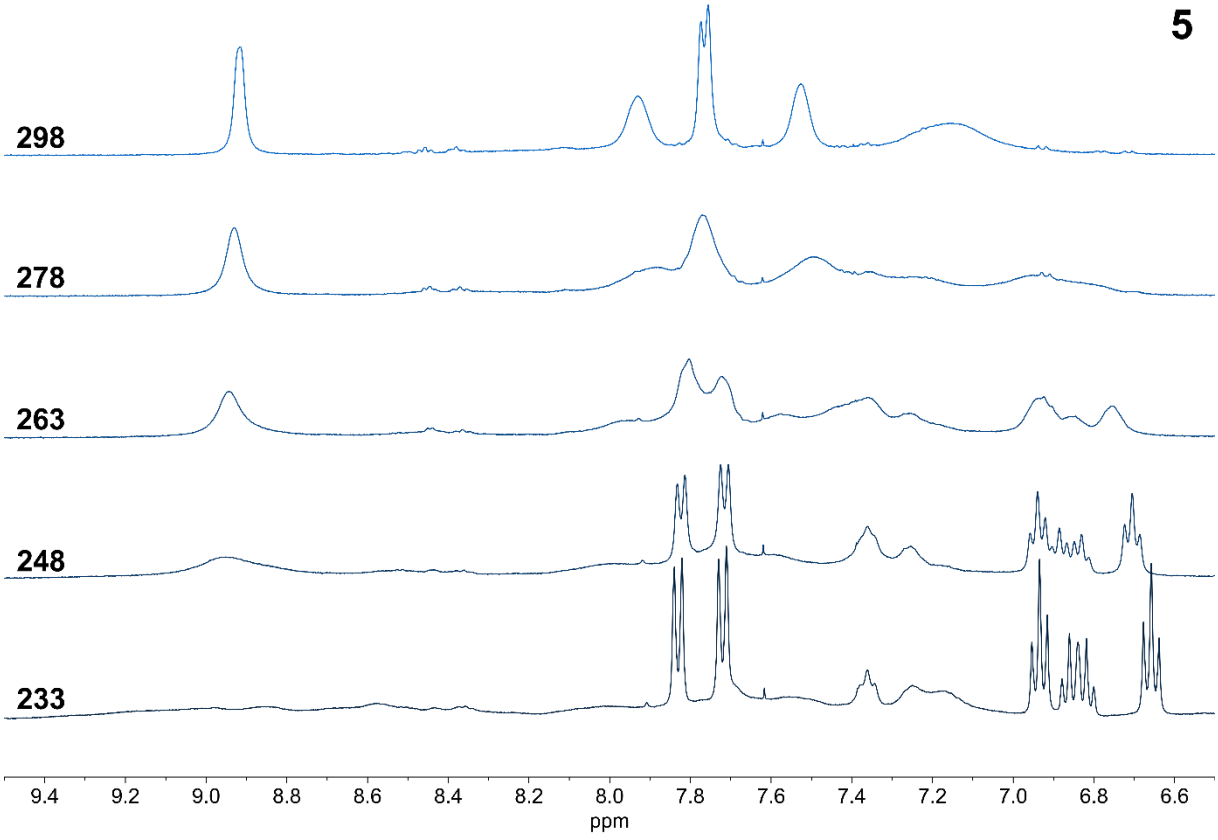


**Figure S6.** Variable temperature $^{1}$H NMR spectra of **5**, $CD_3CN$, aromatic region. The temperature is indicated in K.

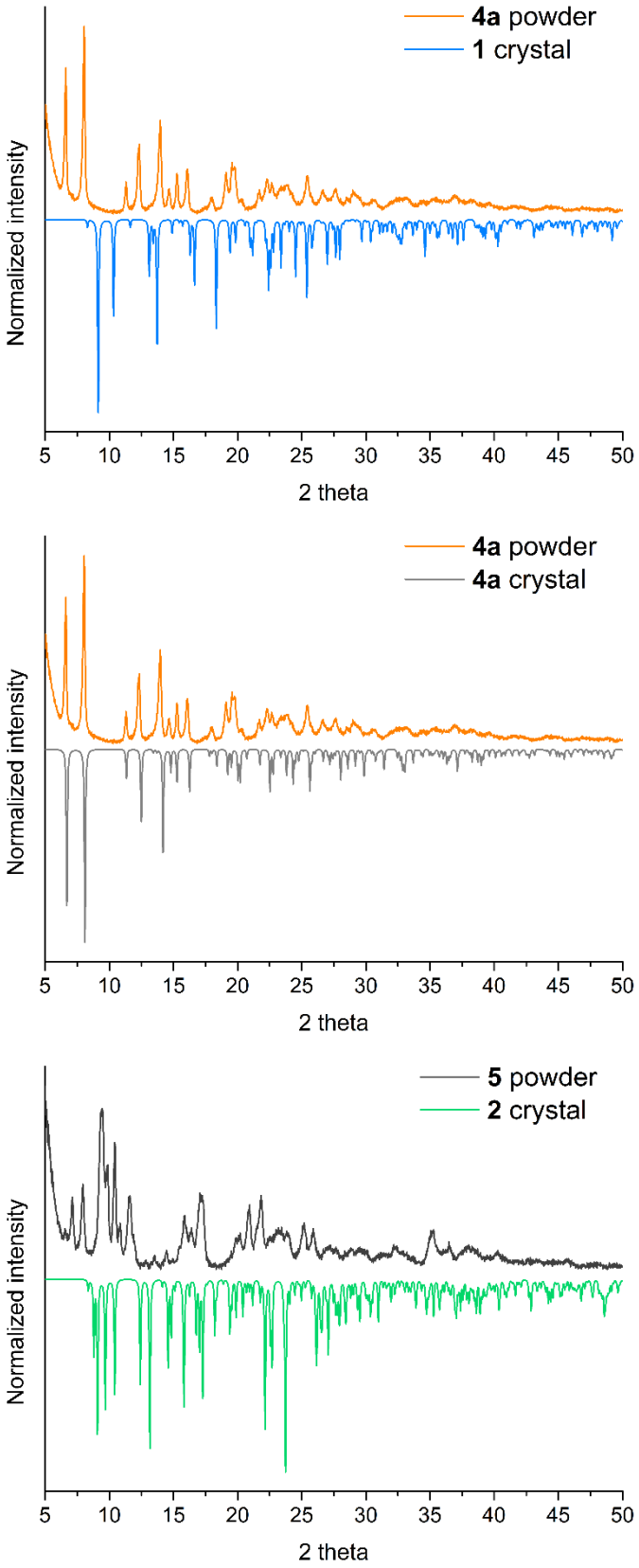


**Figure S7.** XRD powder patterns for **1**, **2**, **4a**, and **5** (powder and single crystal).

**Table S2.** Binding energies (eV) of peaks in XPS spectra of **1**, **2**, **4a**, and **5**.

| Element | Level | 1 | 2 | 4a | 5 |
|---|---|---|---|---|---|
| C | 1s | 284.4 | 284.4 | 284.7 | 284.5 |
| N | 1s | 398.7 | 398.8 | 399.6 | 399.5 |
| P | $2p^{*}$ | 131.0 | 131.4 | 131.8 | 131.8 |
| Au | $4f_{5/2}$, $4f_{7/2}$ | 88.3, 84.6 | 88.5, 84.8 | 88.8, 85.1 | 88.8, 85.1 |
| Cu | $2p_{1/2}$, $2p_{3/2}$ | – | – | 952.4, 932.5 | 952.3, 932.5 |
| B | 1s | – | – | 189.3 | 189.4 |
| F | 1s | – | – | 685.3 | 685.2 |

* Unresolved combination of $2p_{1/2}$ and $2p_{3/2}$ components.

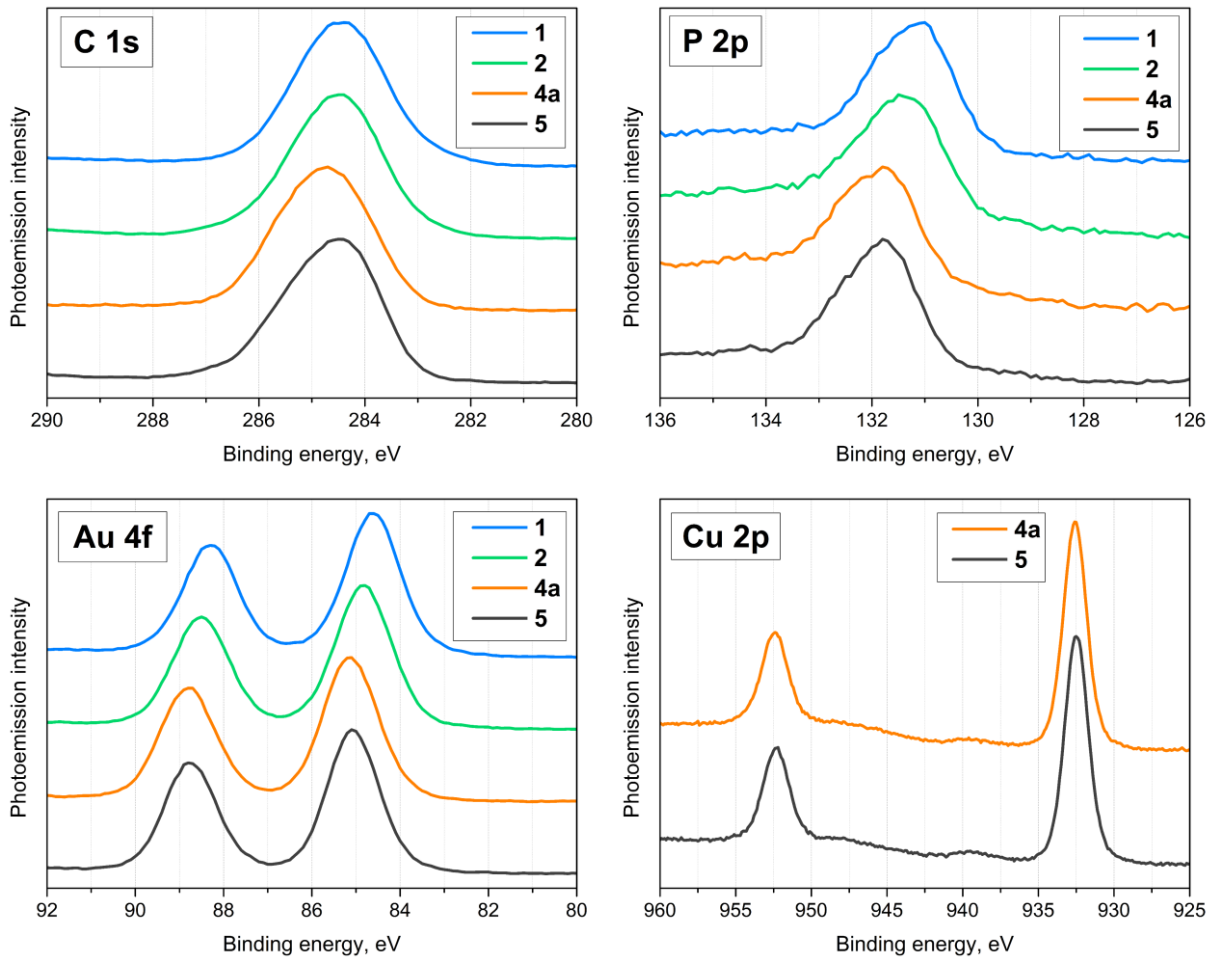


**Figure S8**. Core-level photoemission spectra of **1**, **2**, **4a**, and **5**.

**Table S3.** Optical properties of **1-5**, $CH_2Cl_2$ solution, $c = 10^{-5}$ M, r.t.

| Compound | $\lambda_{abs}$, nm ($\varepsilon$, $10^4$ $cm^{-1}M^{-1}$) |
|---|---|
| **1** | 241(2.33), 260$^{sh}$(2.54), 269(2.90), 283(2.43), 294$^{sh}$(1.35) |
| **2** | 259(1.71), 267$^{sh}$(1.52), 274$^{sh}$(0.89) |
| **3** | 242(4.97), 265$^{sh}$(6.70), 274(7.40), 288(7.00), 295$^{sh}$(6.15), 335(0.24) |
| **4**$^{\#}$ | 237(2.85), 257$^{sh}$(2.67), 267(3.32), 282(2.75), 291$^{sh}$(1.49), 379(0.04) |
| **4** | 245$^{sh}$(2.66), 262(3.17), 270$^{sh}$(3.05), 290$^{sh}$(1.39), 300$^{sh}$(1.28), 385(0.23) |
| **5**$^{\#}$ | 257(1.95), 263$^{sh}$(1.79), 272$^{sh}$(1.17), 373(0.05) |
| **5** | 261(2.40), 270$^{sh}$(1.91), 301(0.48), 386(0.22) |

$^{\#}$ NCMe solution.

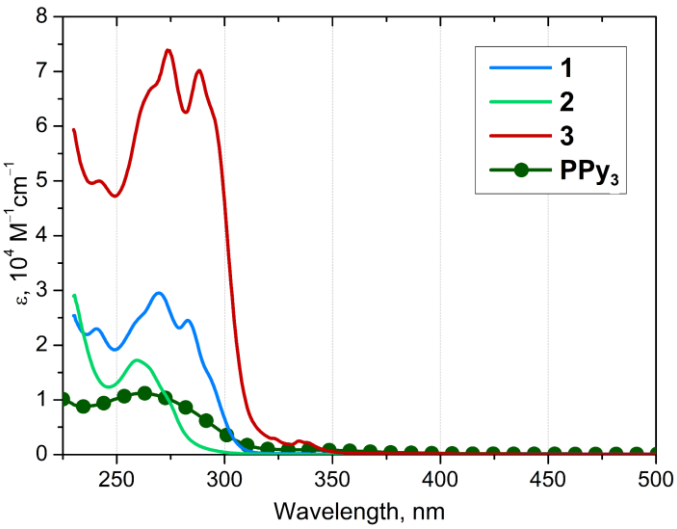


**Figure S9.** UV-Vis absorption spectra of free $PPy_3$ and **1-3**, $CH_2Cl_2$, $c = 10^{-5}$ M, r.t.

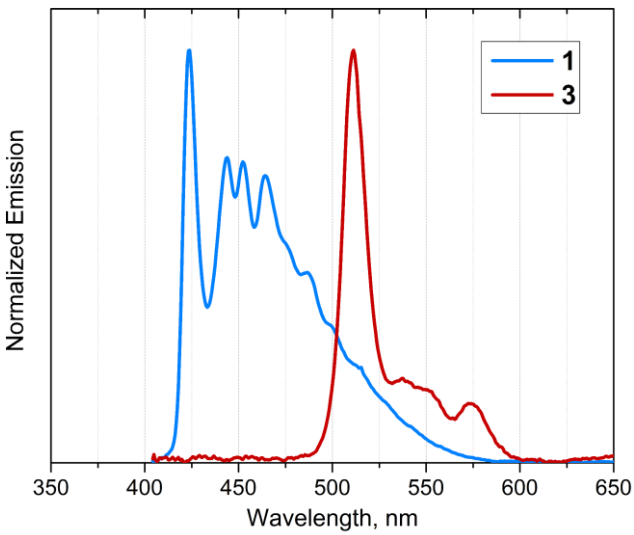


**Figure S10.** Emission spectra of **1** and **3** in the solid state, r.t.

**Table S4.** CIE 1931 Colour coordinates of **1**, **3**, **4a**, and **5** emission in solid state.

| | **1** | **3** | **4a** | | **5** | |
|---|---|---|---|---|---|---|
| | | | r.t. | 77 K | r.t. | 77 K |
| X | 0.1447 | 0.2084 | 0.4170 | 0.4213 | 0.3926 | 0.4283 |
| Y | 0.1213 | 0.6574 | 0.5294 | 0.5592 | 0.5617 | 0.5570 |

* Colour coordinates were calculated using Osram LED ColorCalculator software:
https://www.osram.us/cb/tools-and-resources/applications/led-colorcalculator/index.jsp

**Table S5.** Photophysical properties of **4a** and **5**, solid state, $\lambda_{exct}$ = 380 nm.

| | **$\lambda_{em}$, nm** | **$\lambda_{exct}$, nm‡** | **Φ, %‡** | **$\tau_i$, ns ($f_i$)*** | | **$\tau_{av}$, ns**** | |
|---|---|---|---|---|---|---|---|
| | | | | **RT** | **77 K** | **RT** | **77 K** |
| **4a** | 554 | 335 | 2 | 93(0.1), 527(0.9) | 107(0.12), 604(0.88) | 521 | 542 |
| **5** | 548 | 332, 402 | < 0.1 | 101(0.12), 568(0.88) | 94.3(0.15), 599(0.85) | 512 | 524 |

‡ Ambient temperature. * Fractional intensity $f_i = a_i\tau_i/\sum(a_i\tau_i)$.

** Average for the double exponential decay $\tau_{av} = (A_1\tau_1^2 + A_2\tau_2^2)/(A_1\tau_1 + A_2\tau_2)$, $A_i$ is weight of the *i* exponent.

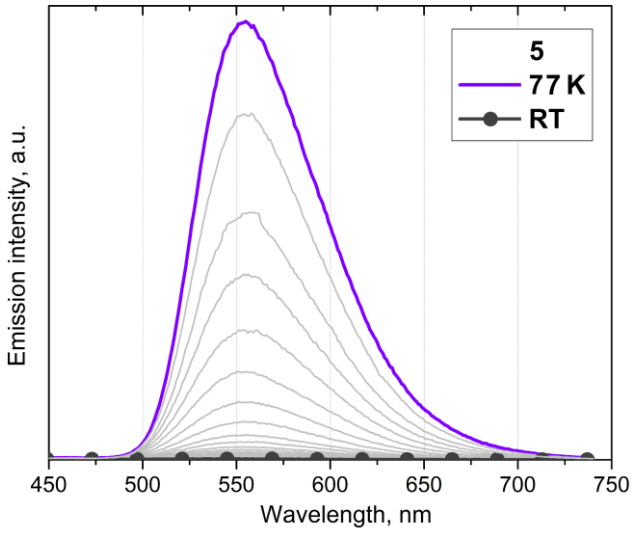


**Figure S11.** Temperature evolution of emission spectra of **5** in the solid state during unprompted heating after treatment by liquid nitrogen, $\lambda_{exct}$ = 380 nm.

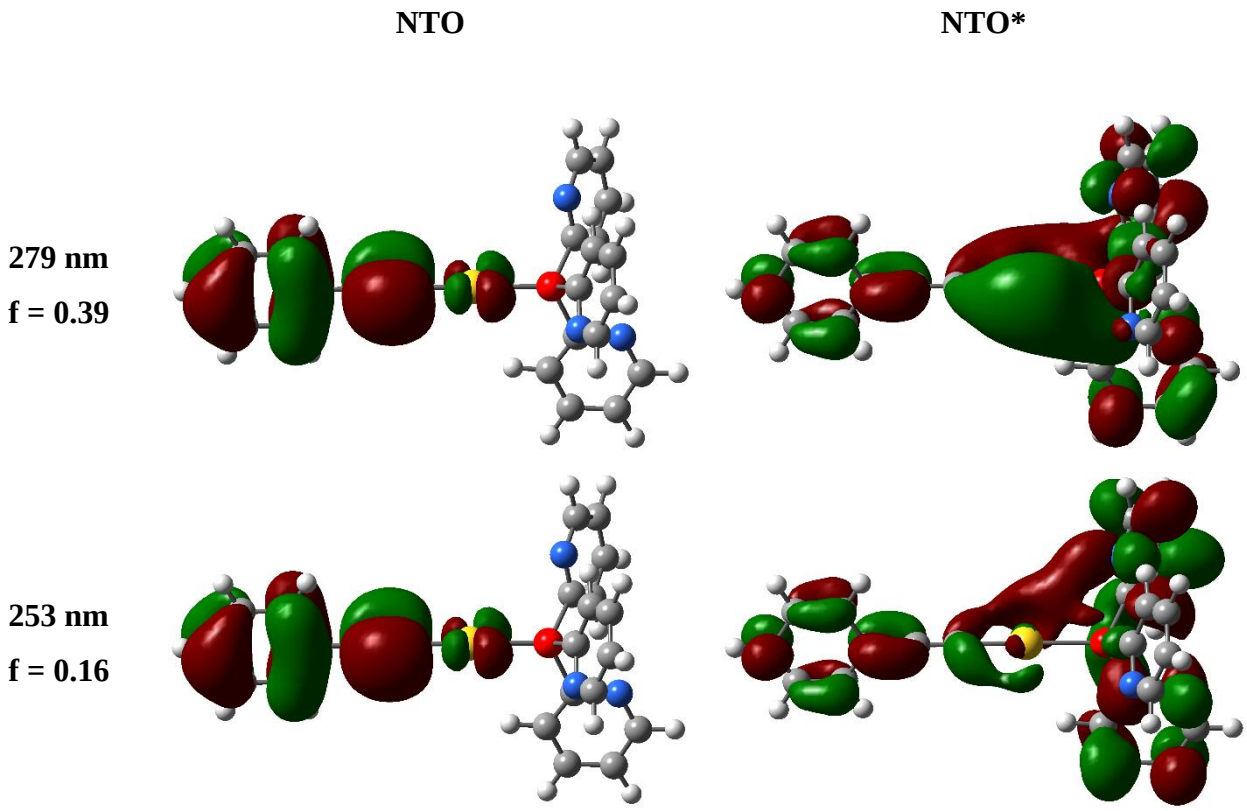


**Figure S12.** Natural transition orbitals (NTOs) describing UV-Vis absorption of the [$PhC_2Au(PPy_3)$] complex (**1**) as obtained from DFT calculations. The calculated wavelength and oscillator strength (f) are provided for each transition together with the most important pair of NTOs.

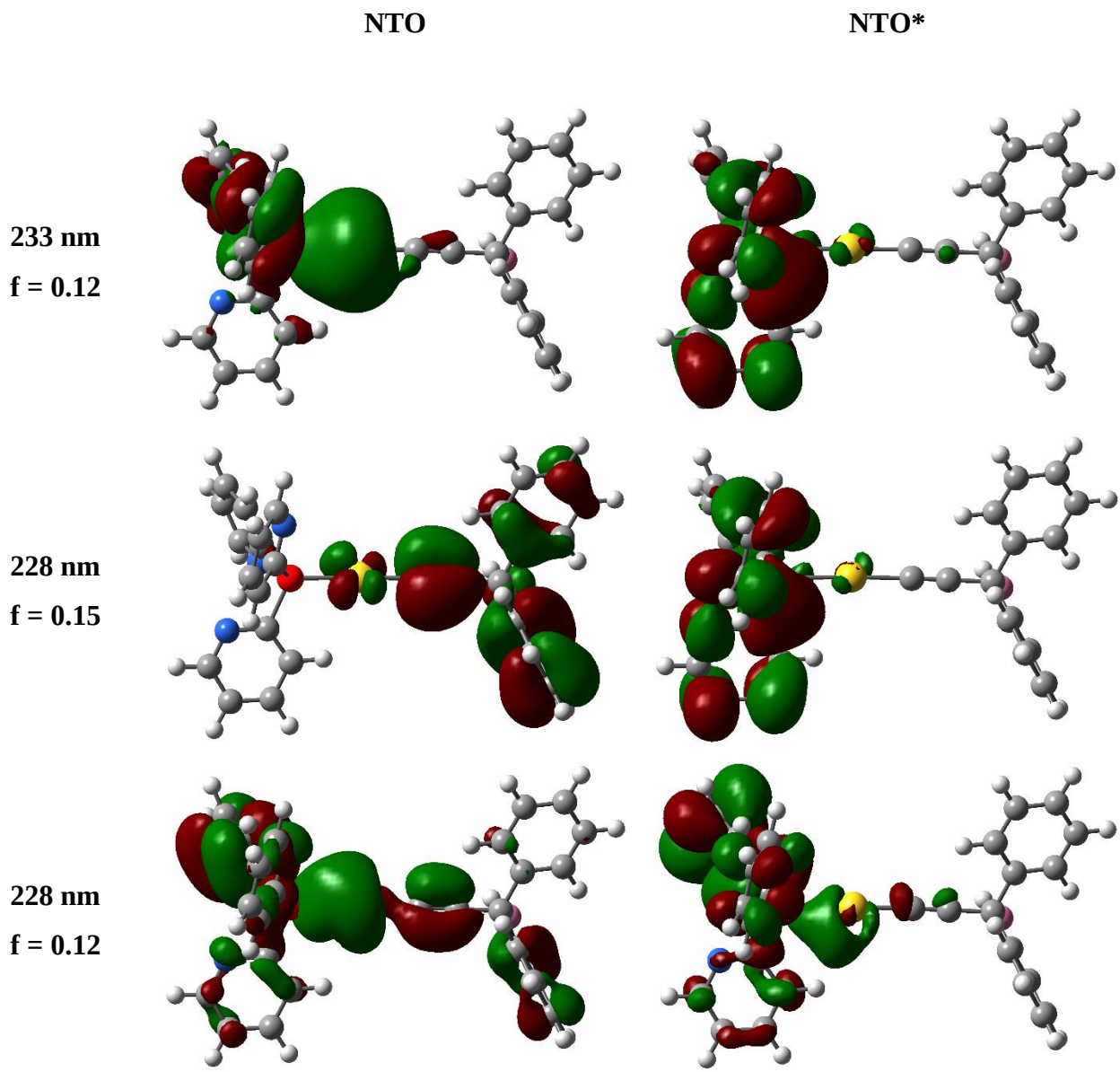


**Figure S13.** Natural transition orbitals (NTOs) describing UV-Vis absorption of the [$Ph_2(OH)CC_2Au(PPy_3)$] complex (**2**) as obtained from DFT calculations. The calculated wavelength and oscillator strength (f) are provided for each transition together with the most important pair of NTOs.

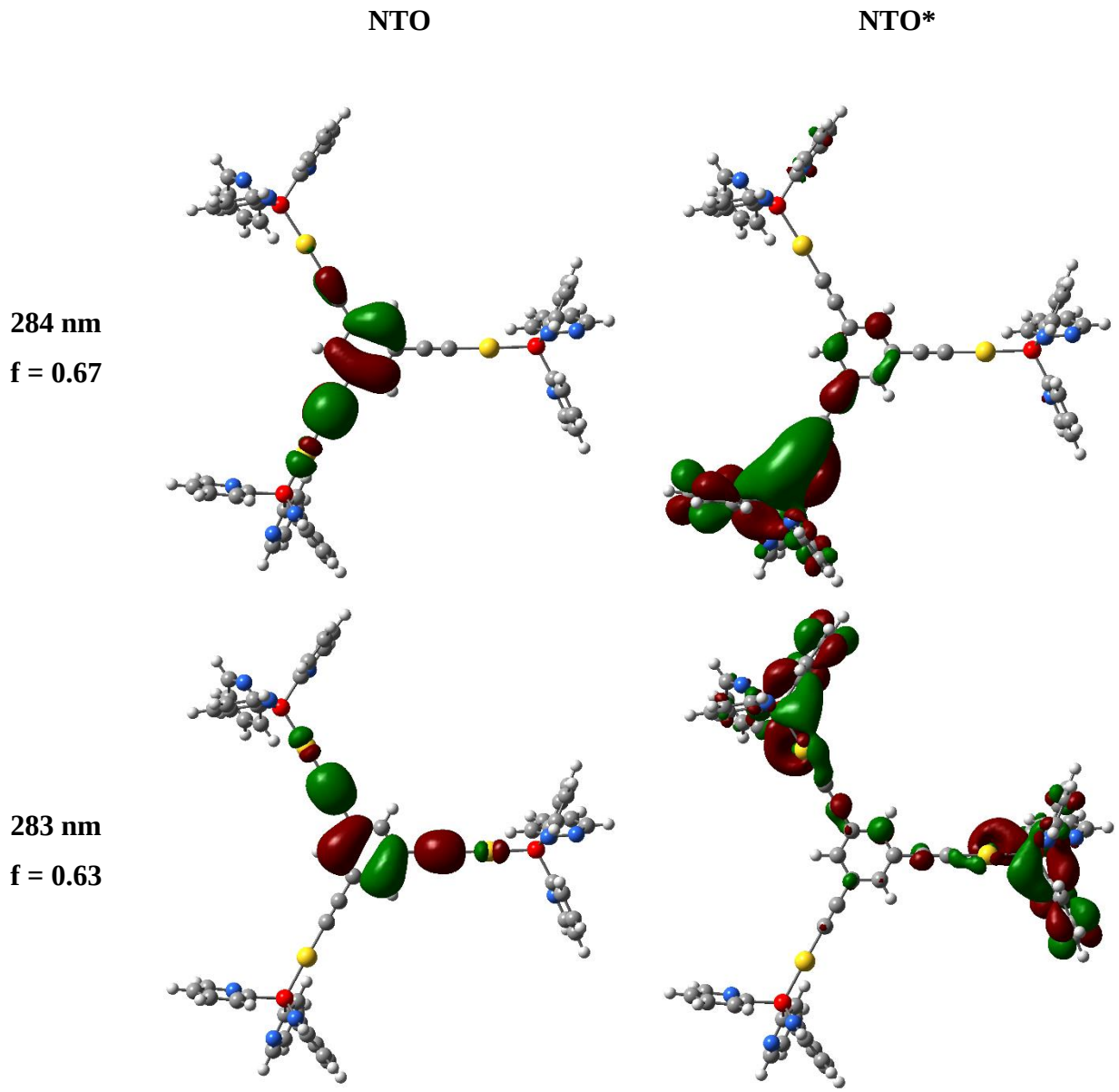


**Figure S14.** Natural transition orbitals (NTOs) describing UV-Vis absorption of the $[C_6H_3(C_2Au(PPy_3))_3]$ complex (**3**) as obtained from DFT calculations. The calculated wavelength and oscillator strength (f) are provided for each transition together with the most important pair of NTOs.

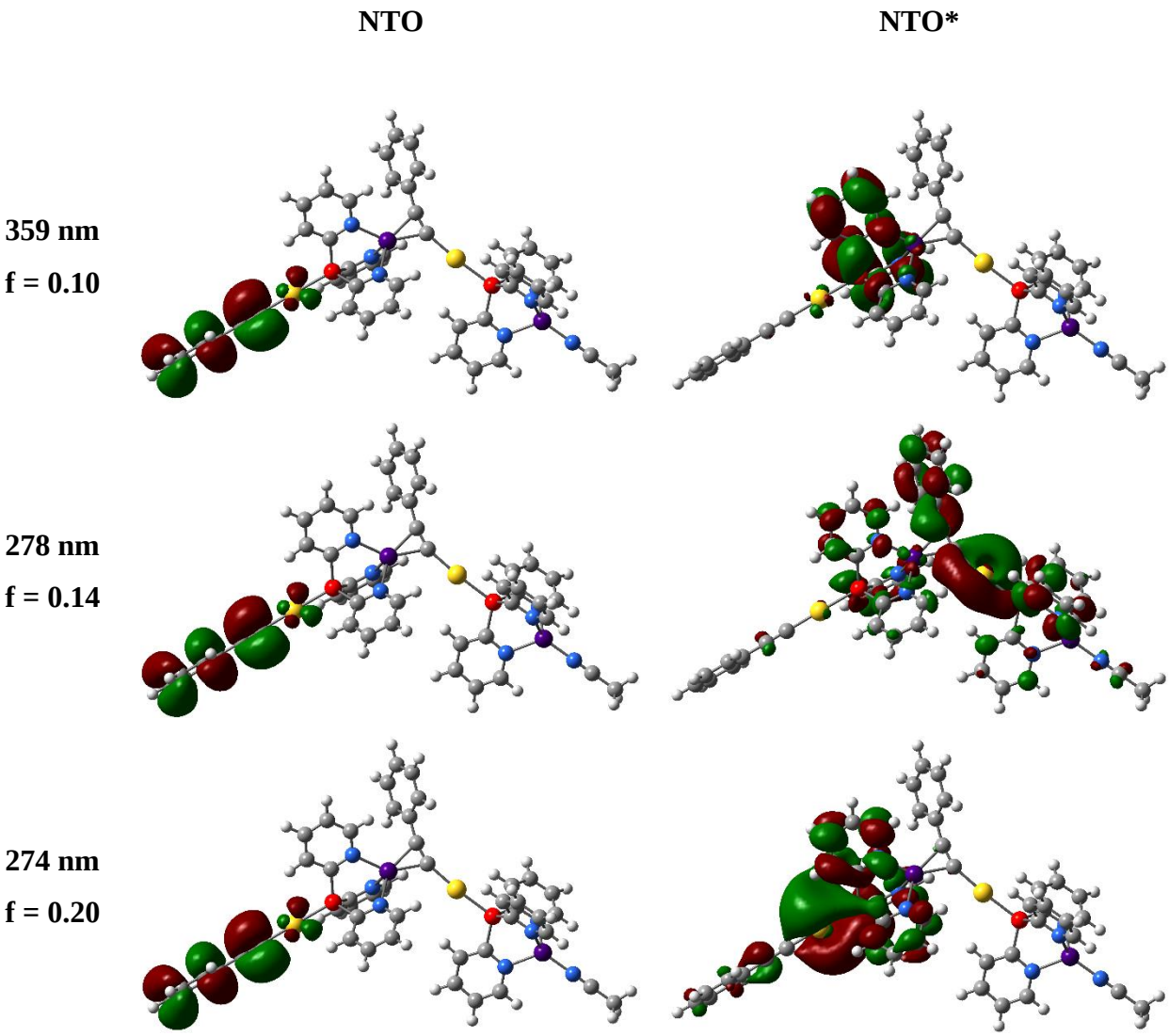


**Figure S15.** Natural transition orbitals (NTOs) describing UV-Vis absorption of the $[PhC_2Au(PPy_3)Cu–PhC_2Au(PPy_3)Cu(CH_3CN)]^{2+}$ model complex (**4**) as obtained from DFT calculations. The calculated wavelength and oscillator strength (f) are provided for each transition together with the most important pair of NTOs.

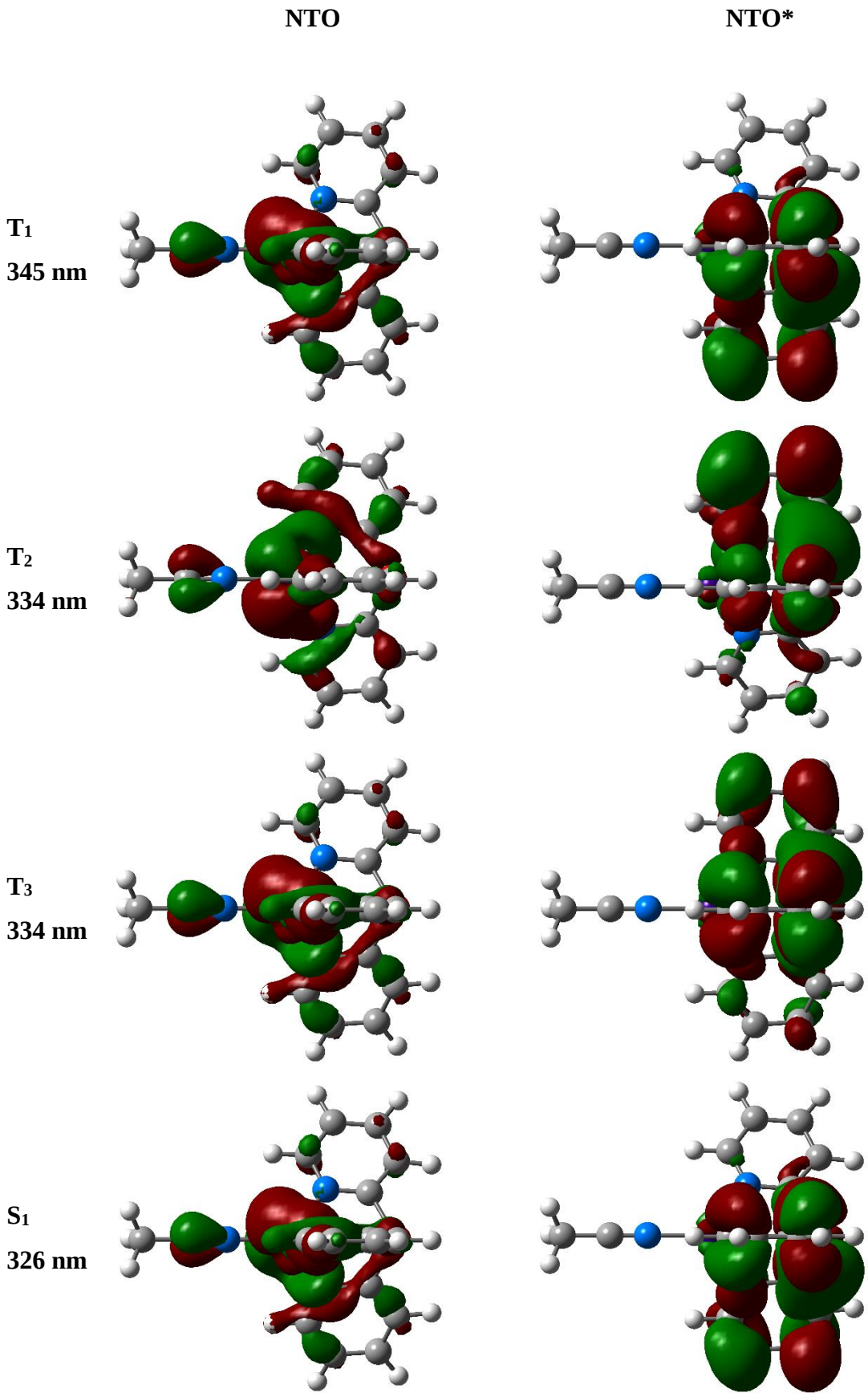


**Figure S16.** Natural transition orbitals (NTOs) for the lowest excited states of the $[Cu(PPy_3)(CH_3CN)]^+$ complex (**Cu**) as obtained from TDDFT calculations. Only the most important pair of NTOs is shown for each state.

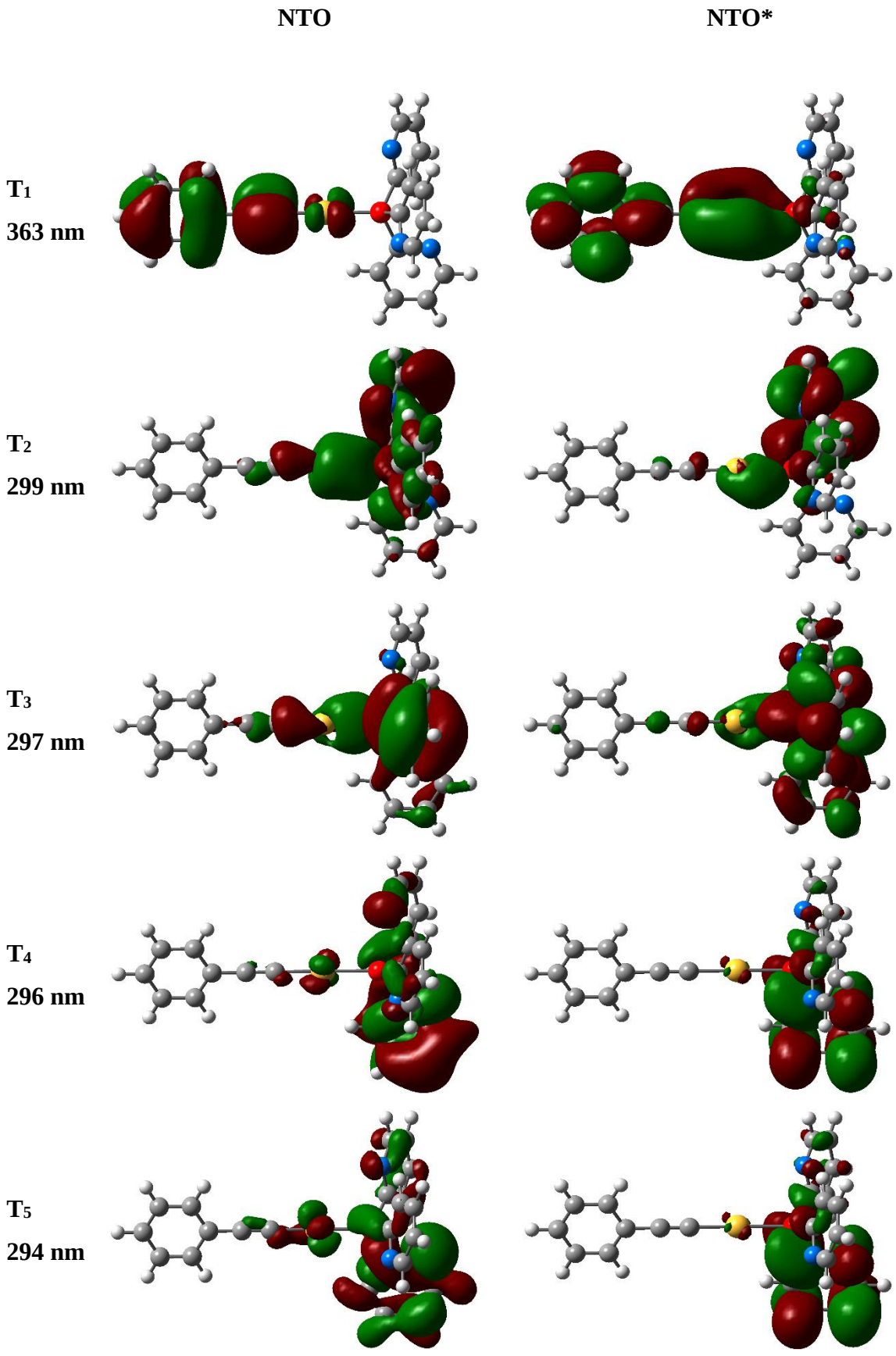


**Figure S17.** Natural transition orbitals (NTOs) for the lowest excited states of the [$PhC_2Au(PPy_3)$] complex (**1**) as obtained from TDDFT calculations. Only the most important pair of NTOs is shown for each state.

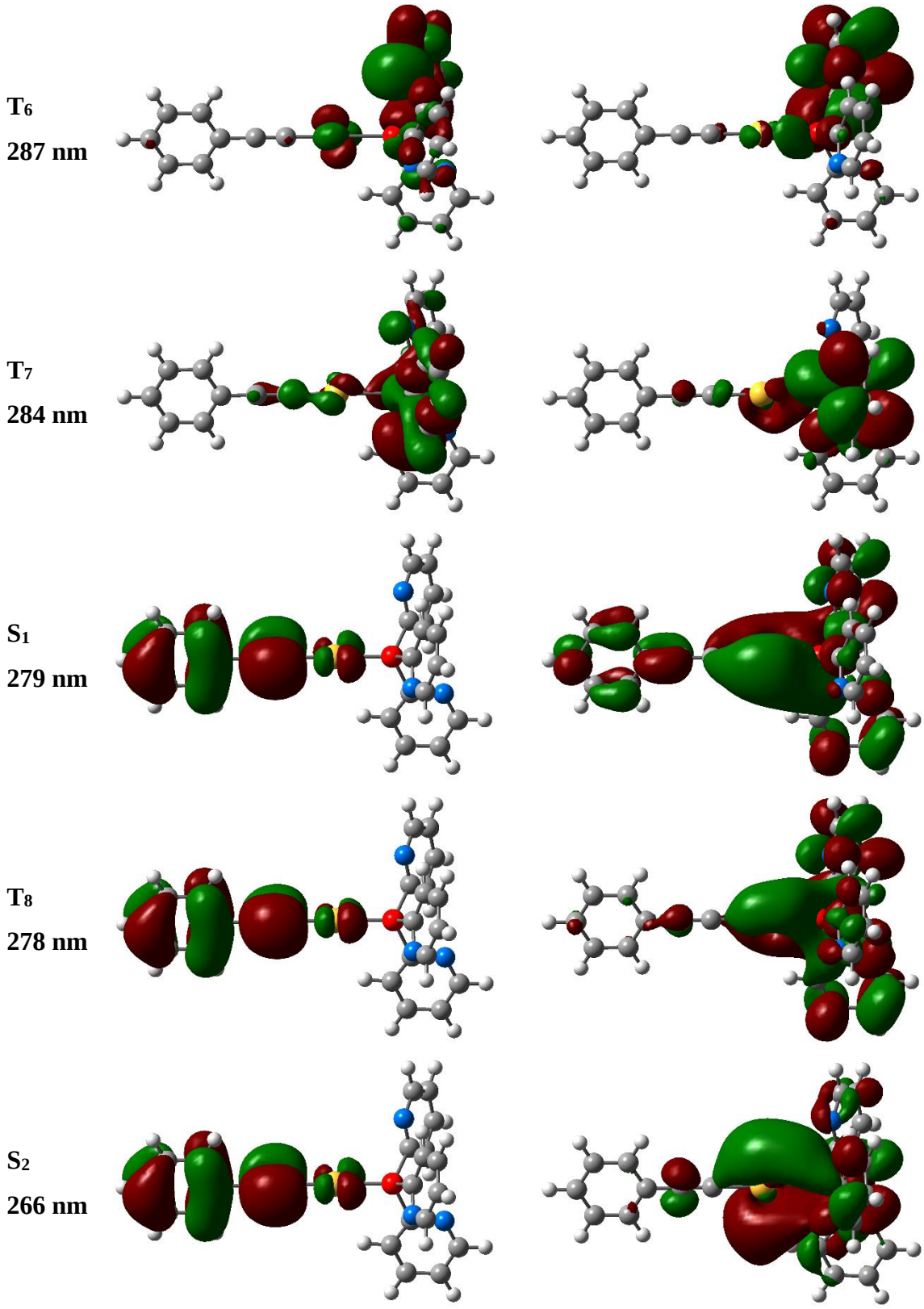


**Figure S17, continued.**

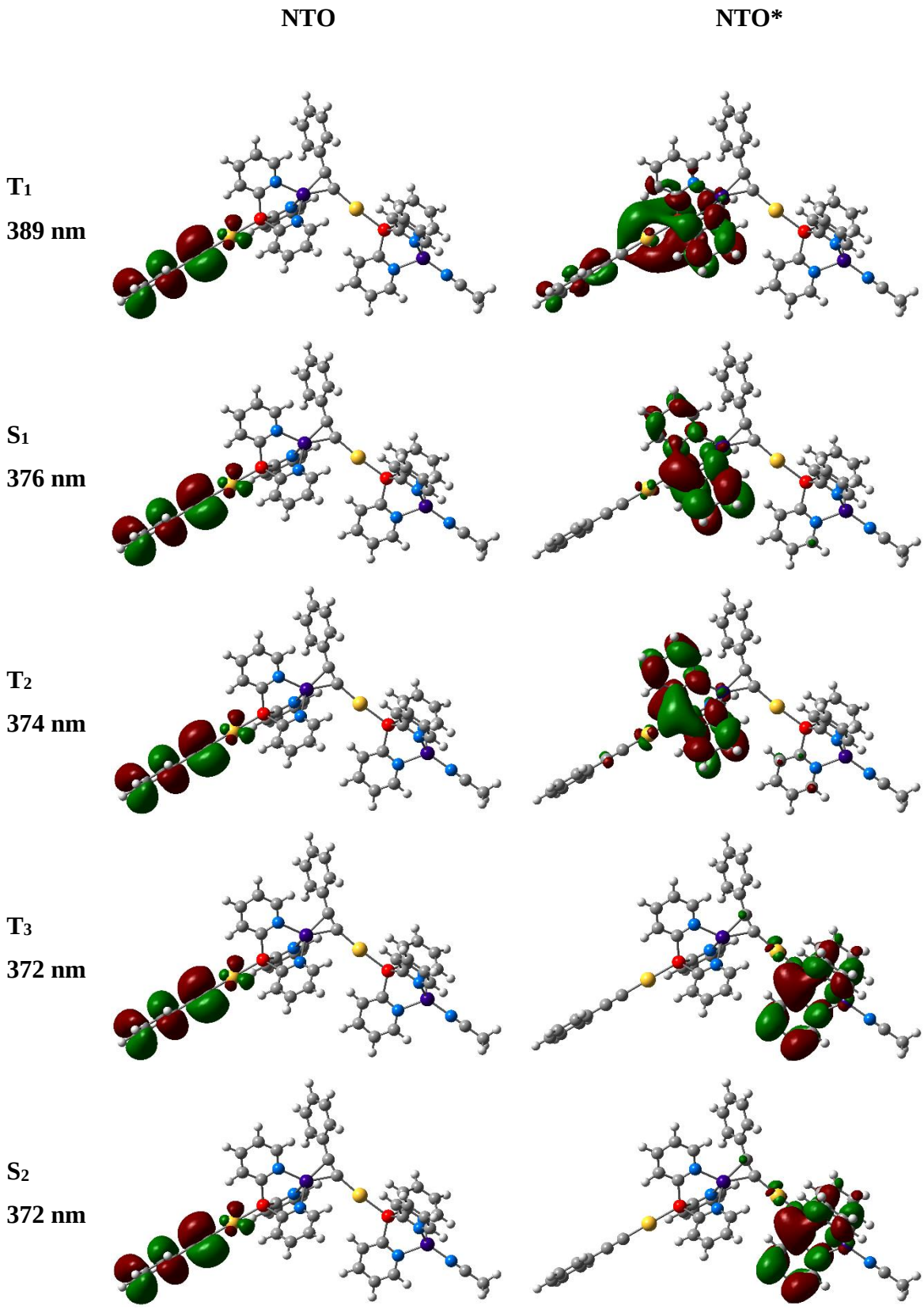


**Figure S18.** Natural transition orbitals (NTOs) for the lowest excited states of the $[PhC_2Au(PPy_3)Cu–PhC_2Au(PPy_3)Cu(CH_3CN)]^{2+}$ complex (**4**) as obtained from TDDFT calculations. Only the most important pair of NTOs is shown for each state.

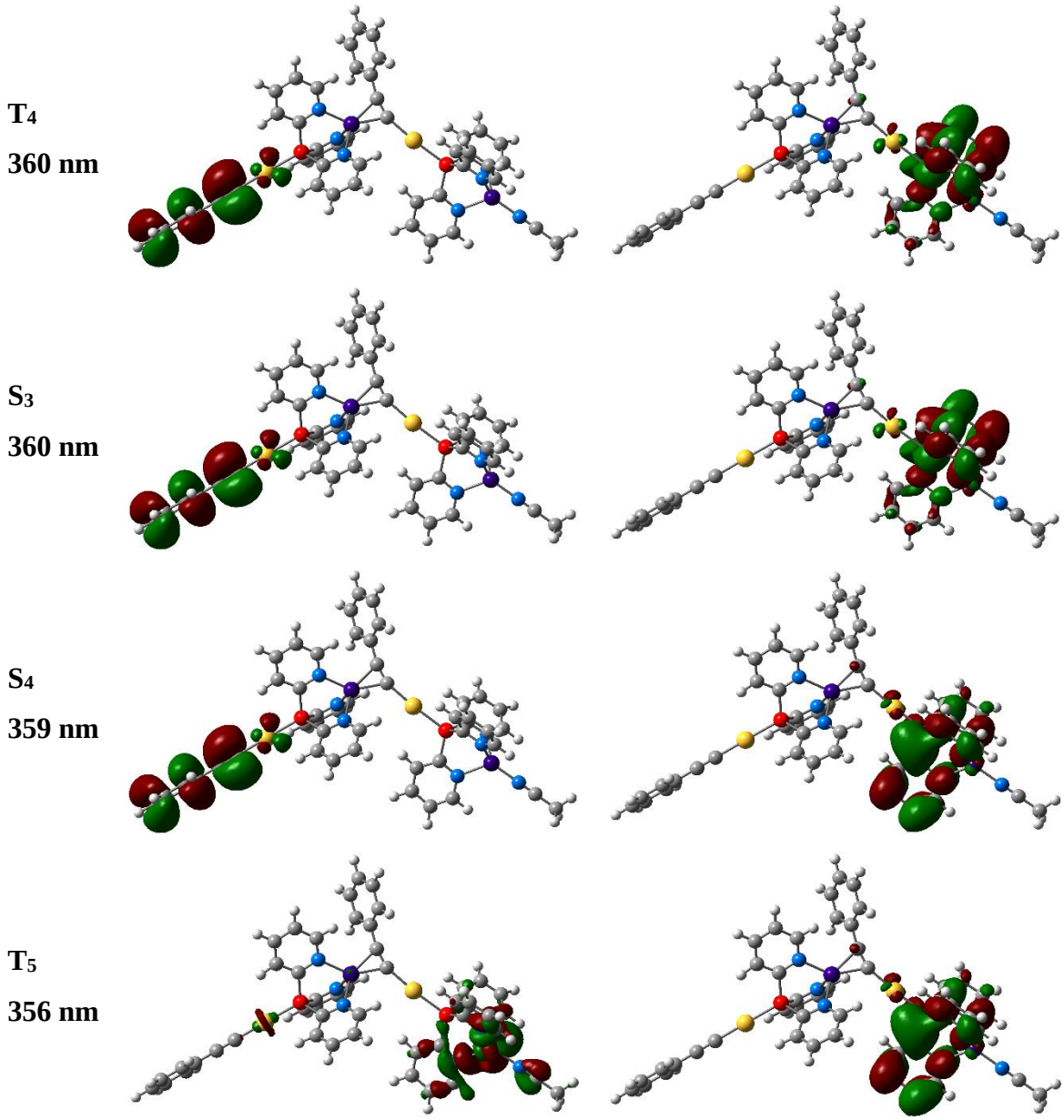


**Figure S18, continued.**